American College of Neuropsychopharmacology

www.nature.com/npp

ARTICLE

Check for updates

Decreased *CNNM2* expression in prefrontal cortex affects sensorimotor gating function, cognition, dendritic spine morphogenesis and risk of schizophrenia

Dan-Yang Zhou[1,2,10], Xi Su[3,4,10], Yong Wu[5,6], Yongfeng Yang[3,4], Luwen Zhang[3,4], Shumin Cheng[3,4], Minglong Shao[3,4], Wenqiang Li[3,4], Zhaohui Zhang[7], Lu Wang[1], Luxian Lv[3,4,8], Ming Li[1,2,9]✉ and Meng Song[3,4]✉

Genome-wide association studies (GWASs) have reported multiple single nucleotide polymorphisms (SNPs) associated with schizophrenia, yet the underlying molecular mechanisms are largely unknown. In this study, we aimed to identify schizophrenia relevant genes showing alterations in mRNA and protein expression associated with risk SNPs at the 10q24.32-33 GWAS locus. We carried out the quantitative trait loci (QTL) and summary data-based Mendelian randomization (SMR) analyses, using the PsychENCODE dorsolateral prefrontal cortex (DLPFC) expression QTL (eQTL) database, as well as the ROSMAP and Banner DLPFC protein QTL (pQTL) datasets. The gene *CNNM2* (encoding a magnesium transporter) at 10q24.32-33 was identified to be a robust schizophrenia risk gene, and was highly expressed in human neurons according to single cell RNA-seq (scRNA-seq) data. We further revealed that reduced *Cnnm2* in the mPFC of mice led to impaired cognition and compromised sensorimotor gating function, and decreased *Cnnm2* in primary cortical neurons altered dendritic spine morphogenesis, confirming the link between *CNNM2* and endophenotypes of schizophrenia. Proteomics analyses showed that reduced *Cnnm2* level changed expression of proteins associated with neuronal structure and function. Together, these results identify a robust gene in the pathogenesis of schizophrenia.

Neuropsychopharmacology (2024) 49:433–442; https://doi.org/10.1038/s41386-023-01732-y

INTRODUCTION

Schizophrenia is a serious disabling public health problem worldwide. Twin studies have revealed strong heritability of schizophrenia [1], and genome-wide association studies (GWAS) have reported multiple genomic loci showing robust statistical associations [2]. Given that majority of GWAS identified risk single nucleotide polymorphisms (SNPs) are in noncoding genomic regions, they are hypothesized to regulate gene expression in relevant cells and tissues [3]. Therefore, integrating GWAS and brain tissues-derived expression resources was applied to characterize genes correlated to genetic risk of schizophrenia [4–7]. The 10q24.32-33 locus is the 4th most significant schizophrenia GWAS locus across the whole genome [2], for example, rs11191580 exhibited genome-wide significant associations with schizophrenia (e.g., $P = 2.23 \times 10^{-8}$ in schizophrenia PGC1 GWAS [8]; $p = 7.07 \times 10^{-16}$ in schizophrenia PGC2 GWAS [9]; $P = 4.47 \times 10^{-23}$ in schizophrenia PGC3 GWAS [2], Fig. 1B). However, whether rs11191580 (or its high LD SNPs) was associated with the expression of any genes remained to be investigated.

Prepulse inhibition (PPI) of acoustic startle reflex is an operational measure of sensorimotor gating that reflect the information processing and filtering function [10], and there is considerable evidence to support sensorimotor gating deficits in schizophrenia patients [11]. In preclinical studies, impairment of PPI is a reliable endophenotype for evaluating animal models relevant to schizophrenia and has become the most influential experimental paradigm for understanding its pathophysiology [12], and murine models of many schizophrenia risk genes exhibited deficits in sensorimotor gating function [13–15]. In addition, accumulating studies indicated abnormal structures and dysfunction of brain areas that engage in cognitive processes, such as prefrontal cortex [16]. Altered dendritic spine morphogenesis and synapse formation in the dorsolateral prefrontal cortex (DLPFC) have been repeatedly observed in schizophrenia patients [17–23], and multiple schizophrenia risk genes have been found to affect dendritic spines, such as *ZNF804A*, *ANK3* and *DISC1* [24–27], suggesting they may contribute to disease susceptibility at least in part *via* modulating dendritic spine structure and function.

[1]Yunnan Key Laboratory of Animal Models and Human Disease Mechanisms, Kunming Institute of Zoology, Chinese Academy of Sciences, Kunming, Yunnan, China. [2]Kunming College of Life Science, University of Chinese Academy of Sciences, Kunming, Yunnan, China. [3]Henan Mental Hospital, The Second Affiliated Hospital of Xinxiang Medical University, Xinxiang, Henan, China. [4]Henan Key Lab of Biological Psychiatry, International Joint Research Laboratory for Psychiatry and Neuroscience of Henan, Xinxiang Medical University, Xinxiang, Henan, China. [5]Research Center for Mental Health and Neuroscience, Wuhan Mental Health Center, Wuhan, Hubei, China. [6]Affiliated Wuhan Mental Health Center, Jianghan University, Wuhan, Hubei, China. [7]Department of Psychiatry, The First Affiliated Hospital of Xinxiang Medical University, Xinxiang, Henan, China. [8]Henan Province People's Hospital, Zhengzhou, Henan, China. [9]KIZ/CUHK Joint Laboratory of Bioresources and Molecular Research in Common Diseases, Kunming Institute of Zoology, Chinese Academy of Sciences, Kunming, Yunnan, China. [10]These authors contributed equally: Dan-Yang Zhou, Xi Su. ✉email: limingkiz@mail.kiz.ac.cn; song.meng.201@163.com

Received: 16 November 2022 Revised: 15 August 2023 Accepted: 31 August 2023
Published online: 15 September 2023

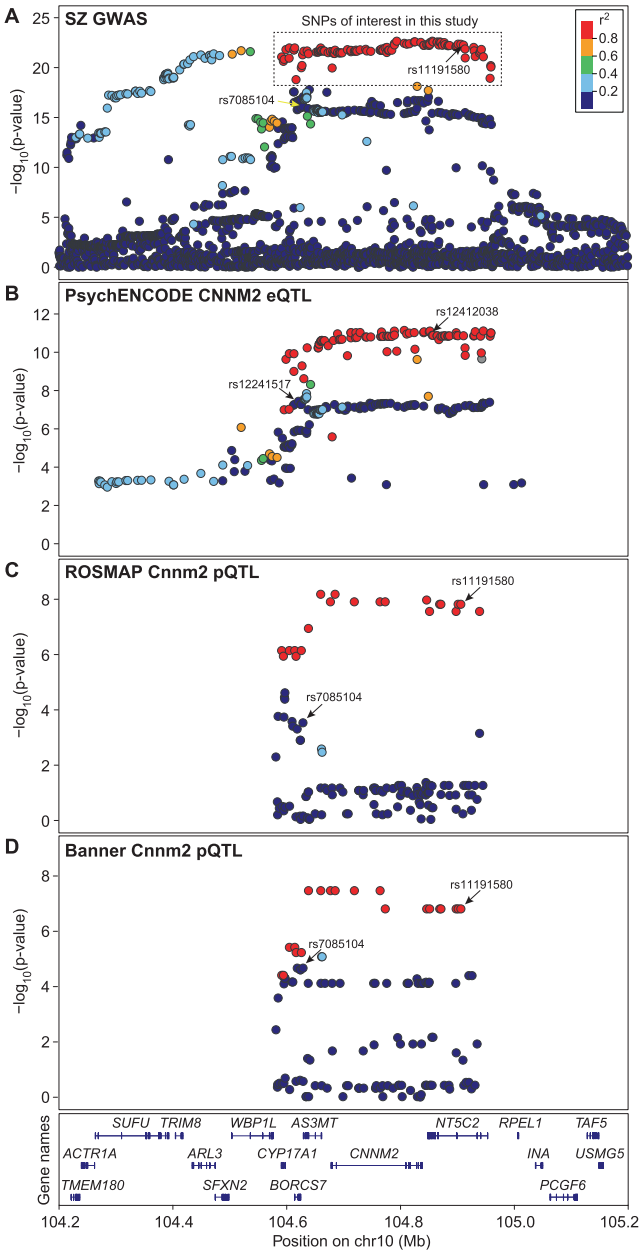

Fig. 1 Genetic and molecular characterizations of 10q24.32-33 GWAS locus. Associations of SNPs spanning 10q24.32-33 region with risk of schizophrenia (SZ) in PGC3 GWAS (**A**), CNNM2 mRNA expression in PsychENCODE dataset (**B**), CNNM2 protein expression in ROSMAP (**C**) and Banner (**D**) datasets, respectively. A physical map of the region is given and depicts known genes within the region, and the LD is defined based on the SNP rs11191580. Rs11191580 and rs7085104 (or its LD-linked SNP rs12241517) were marked in the figure.

Therefore, risk gene identification for schizophrenia usually require demonstration that they affect the aforementioned endophenotypes. Here, through analyzing DLPFC mRNA and protein quantitative trait loci (QTL) in combination with other integrative analyses, we have identified an essential schizophrenia risk gene *CNNM2* (encoding a magnesium transporter) in the prominent 10q24.32-33 schizophrenia GWAS locus. The risk SNPs predicted lower *CNNM2* mRNA and protein levels in human DLPFC, and reduced *Cnnm2* expression led to compromised sensorimotor gating function and impaired cognition in mice as well as altered dendritic spine morphogenesis.

METHODS AND MATERIALS

Schizophrenia GWAS dataset

The Psychiatric Genomics Consortium (PGC3) has conducted GWAS of schizophrenia including 69,369 cases and 236,642 controls [2]. We retrieved the GWAS summary statistics from https://www.med.unc.edu/pgc/download-results. Details of sample description and GWAS analyses can be found in the original study.

DLPFC eQTL and pQTL datasets

We utilized PsychENCODE expression quantitative trait loci (eQTL) data to examine the impact of risk SNPs on mRNA expression in human DLPFC tissues of 1387 European individuals [28]. Briefly, the eQTL was calculated with FastQTL [29] using top 5 genotyping principal components, sequencing platform, sequencing protocol, sex and 50 factors identified by Probabilistic Estimation of Expression Residuals method [30] as covariates. The mapping window was defined as 1 Mb from the transcription start site and nominal *p*-values were generated for each SNP-gene pair using a linear regression model. The eQTL summary data in BESD format could be downloaded at https://cnsgenomics.com/software/smr.

For ROSMAP protein quantitative trait loci (pQTL) data, human DLPFC proteomes were generated using the isobaric tandem mass tag and mass spectrometry of European individuals from the ROSMAP project. After quality control, 376 subjects with both proteomic and genetic data were proceeded for the pQTL analysis. PLINK [31] was used to estimate the pQTLs by linear regression within a 100 kb window around the protein-coding gene. Clinical diagnosis, the first ten genetic principal components, and ten surrogate variables was used as covariates during the pQTL mapping. The DLPFC pQTL summary data was downloaded from the AMP-AD Knowledge Portal (https://doi.org/10.7303/syn23627957) [32, 33].

For Banner pQTL data, human DLPFC proteomes of European participants from the Banner Sun Health Research Institute were generated using the same approach as described for the ROSMAP proteomes with minor differences. After quality control, 152 subjects with both proteomic and genetic data were proceeded for the pQTL analysis. The DLPFC pQTL summary data was downloaded from the AMP-AD Knowledge Portal (https://doi.org/10.7303/syn23627957) [32, 33].

SMR integrative analyses

The summary data-based Mendelian randomization (SMR) was applied to identify risk genes using the summary statistics from schizophrenia GWAS and QTL datasets [34]. Like Mendelian randomization, the SMR use genetic variants (SNPs) as instrumental variable to test for the causative effect of an exposure (in this study, in refers to gene expression) on an outcome (schizophrenia). We respectively integrated the PsychENCODE DLPFC eQTL datasets [28] as well as ROSMAP and Banner DLPFC pQTL datasets [32, 33] with the schizophrenia PGC3 GWAS [2] to perform the SMR analyses (version 1.03). The threshold of eQTL/pQTL *P*-value in the SMR analysis was set to be 5.00×10^{-4} and default values of other parameters were used. We also used its accompanying heterogeneity in dependent instruments (HEIDI) test to examine whether the causal role of a gene detected by SMR was due to linkage disequilibrium ($P_{HEIDI} < 0.05$). About 10,000 genes retrieved from the DLPFC eQTL datasets were included in the SMR analysis [28], and therefore genes with $P_{SMR} \le 5.00 \times 10^{-6}$ (after multiple testing correction according to number of tested genes, 0.05/10,000) and $P_{HEIDI} > 0.05$ were considered as potential susceptibility genes associated with genetic risk of schizophrenia. For SMR analysis with DLPFC pQTL datasets [32, 33], about 1000 proteins were included, and $P_{SMR} \le 5.00 \times 10^{-5}$ plus $P_{HEIDI} > 0.05$ were considered as risk proteins significantly associated with schizophrenia genetic risk.

Gene expression analyses in human tissues and cells

The GTEx (release v8) RNA-Seq results of 17,382 samples out of 53 tissues from 948 donors [35] were downloaded from https://www.gtexportal.org/home/. Single cell RNA-seq (scRNA-seq) data, published by ref. [28] by merging and re-analyzing results of three single cell studies [36–38], which included both excitatory and inhibitory neurons, major nonneuronal types (e.g., microglia and astrocytes), and additional cell types associated with development, was downloaded from http://resource.psychencode.org.

Cnnm2-shRNA sequence

Knockdown of rat and mouse *Cnnm2* was achieved by short hairpin RNA (shRNA). The shRNA sequence targeting *Cnnm2* exon 4 was 5′-GCCCGTAGACTACTTCGTC-3′ and a non-specific target sequence (5′-GATTTGCTGTTCGCCCAAG-3′) was employed as negative control.

Adeno-associated virus (AAV) package and purification

The shRNA sequences were constructed into the pAAV-CAG-tdTomato vector (Addgene, #59462) and Sanger sequencing was used to ensure the correct construction. These shRNA sequences were incorporated into plasmid including AAV2 inverted terminal repeat sequence, which were used for packaging adeno-associated virus (AAV). The plasmid encoding AAV-DJ capsid (pAAV-DJ-N589X, Addgene #130878) and the helper plasmid (pAdDeltaF6, Addgene #112867) were also used for AAV packaging; the resulting AAV were named AAV-*Cnnm2*-shRNA (expressing *Cnnm2*-shRNA) and AAV-Control-shRNA (expressing Control-shRNA).

Stereotaxic surgery and virus injection in mice

All animal experiments were performed following the guidelines (developed by the National Advisory Committee for Laboratory Animal Research) for ethical conduct in the care and use of animals, and the protocols were approved by the Animal Ethic Committee of Kunming Institute of Zoology prior to the study. 6–7 weeks wild-type C57BL/6J male mice purchased from GemPharmatech Co., Ltd. (Nanjing, China) were housed in groups of 3–5 with free access to food and water in a temperature-controlled room (23 ± 2 °C) with 50–60% relative humidity and 12 h light/dark cycle. The mice were acclimated to the environment for a week, then stereotaxic surgery was performed following a previous study with minor modifications [39]. Mice were randomly divided into two groups for injection of AAV-*Cnnm2*-shRNA and AAV-Control-shRNA. Mice were anesthetized by inhaling isoflurane and mounted on a stereotaxic frame. For intra-mPFC viral injection, AAV-*Cnnm2*-shRNA and AAV-Control-shRNA were respectively injected bilaterally into the mPFC at a titer of 5×10^{12} vg/mL, based on the antero-posterior and lateral coordinates assigned to the prelimbic cortex (PrL, AP = 1.80 mm, ML = ± 0.40 mm, DV = −2.30 mm from the bregma) of male C57BL/6J mice (300 nL per side at 1 nL/s). Behavioral tests were performed 4 weeks after AAV injection. The AAV-infected cells in the mPFC expressed a red fluorescent protein. The injection site was verified through detecting the location of red fluorescent protein at the end of the behavioral experiment.

RNA extraction and real-time quantitative PCR (RT-qPCR)

The mice were euthanized using a CO_2 chamber 4 weeks after virus injection, and mPFC tissues were immediately dissected under stereoscope on ice ($n = 4$, each group). The tissues were snap frozen in liquid nitrogen after dissection, and total RNA was isolated with TRIzol reagent. The cDNA was generated with the RevertAid First Strand cDNA Synthesis Kit and real-time quantitative PCR (RT-qPCR) was performed using FastStart Universal SYBR Green Master. Primers for amplification of mice *Cnnm2* were 5′-TCCGGATGACTGTACTCCCT-3′ (forward) and 5′-GTTCACTCGCTGCACAATGG-3′ (reverse), and primers for amplification of mice *Gapdh* were 5′-TGTGTCCGTCGTGGATCTGA-3′ (forward) and 5′-TTGCTGTTGAAGTCGGAGGAG-3′ (reverse).

Behavioral tests

Mice behavioral tests were performed following previous studies with minor modifications [40]. All behavioral procedures were conducted during the light periods between 9:00 am and 18:00 pm in the behavioral room, and less stressful tests were performed prior to more stressful ones. Before testing, mice were habituated to the behavioral room and the investigator, who was blind to the treatment, for a week. In each experiment, the mice from two groups were tested alternately. The movement of mice in these tests was tracked and recorded with the SuperMaze and VisuTrack software (Shanghai XinRuan Information Technology Co., Shanghai).

Open filed test. The open field device (40 cm × 40 cm × 40 cm, L × W × H) was divided into central and corner areas. At the beginning of the experiment, the mice were placed in the corner area facing the wall and allowed to explore freely for 5 min. The distance traveled and time spent in different areas were recorded and analyzed.

Rotarod test. On days 1–3, mice were trained to run on the rotarod and rotated at a constant speed of 10 rpm/min for 5 min per day. On day 4, the mice were placed on the rotarod and rotated from 4 to 40 rpm/min at a random acceleration speed within 5 min. The mice were tested three times at 30 min intervals, and the latency to fall was recorded for each time.

Novel object recognition. The open field apparatus (40 cm × 40 cm × 40 cm, L × W × H) was used for this experiment. On the first day, mice were allowed to explore the apparatus freely for 5 min. On the second day, mice were allowed to explore two identical objects (familiar object, wooden, triangular, purple, 3 cm × 3 cm × 3 cm) for 10 min (training session). After an intertrial interval of 6 h, one of the two objects was replaced with a new one (novel object, wooden, square, red, 3 cm × 3 cm × 3 cm) and mice were allowed to explore the two different objects for 10 min (test session). To avoid the influence of the spatial bias of mice for a certain position, the position of the familiar object and the novel one was alternated between trials in test session. The time mice spent respectively in exploring the two objects (with the nose point within 2 cm of the object) in training session and test session was record. The discrimination rate was calculated as (the exploring time for novel object − the exploring time for familiar object)/(the exploring time for novel object + the exploring time for familiar object).

Y-maze for spatial reference memory. A Y-shaped maze composed of three identical closed arms (35 cm × 5 cm × 15 cm, L × W × H,) at an angle of 120° between each other was used for this test. These arms were defined respectively as arm A, B and C, and different shaped signs were attached to the ends of arm B and C. This experiment consists of two trials, training session and test session, with an intertrial interval of 2 h. On the training session, mice were placed into arm A with the arm C (which was defined as the novel arm) closed off, and were allowed to explore freely in arm A and B for 10 min. On the testing session, the arm C was opened on and mice were allowed to explore all the arms freely for 5 min. The time spent in the novel arm and entries to the novel arm were record and used to assess the spatial reference memory of mice.

Y-maze spontaneous alternation. This test was conduct with the Y-maze apparatus above mentioned. At the beginning, mice were placed at the terminal of one arm facing the center of the maze and allowed to explore freely for 8 min. The sequence of arm entries was recorded, and three consecutive entries to the different arms (including ABC, BCA, CAB, ACB, BAC, CBA) were defined as once spontaneous alternation. The spontaneous alternation rate was calculated as follow: the number of spontaneous alternation / (total number of arm entries – 2).

Prepulse inhibition. The PPI test was performed using an acoustic startle reflex measurement system (VisuStartle, Shanghai XinRuan). The test mouse was put into a plastic restrainer which was placed on a gravity sensing platform in a soundproof chamber for 5 min for preadaptation. 62 dB background noise was presented in the chamber throughout the experiment. In session 1, mice were exposed to 120 dB startle pulse lasting 40 ms with random intervals (the average interval was 15 s) for 10 times. In session 2, mice were exposed to five different trials: various intensity of prepulse (74 dB, 78 dB, 86 dB) only, 120 dB startle pulse only, 74 dB prepulse and 120 dB startle pulse, 78 dB prepulse and 120 dB startle pulse, 86 dB prepulse and 120 dB startle pulse. The prepulse (20 ms) was given 100 ms before the startle pulse (40 ms). In this session, each trial was repeated for 10 times and presented in pseudorandom order at random intervals (the average interval was 15 s). The startle responses of mice were recorded, and the percent of PPI was calculate as 100 – (average of startle response to prepulse)/(average of startle response to startle pulse) × 100 to evaluate the function of sensorimotor gating.

Statistical analysis. For normally distributed data evaluated by Shapiro-Wilk test, two-tailed student's *t* tests were used to assess the difference between two groups. For comparing the percent of PPI in the PPI test, repeated-measures t-test was used. All data were analyzed using GraphPad Prism software and were presented as mean with standard error of mean (mean ± SEM), and $P \leq 0.05$ was considered as significant.

Rat cortical neuronal cultures and dendritic spine analyses

Wild-type Sprague Dawley rats were bred with free access to food and water in a temperature-controlled (23 ± 2 °C) room with 50–60% relative humidity and 12 h light/dark cycle. The neuronal culture protocols were following our previous studies [41, 42]. Briefly, pregnant Sprague Dawley

rats (E18/19) were euthanized using a CO_2 chamber. Cortices from embryos were dissected and treated with DNase I and Papain, followed by gently trituration to obtain single-cell suspensions. The dissociated neurons were then seeded in six well culture-plates, which were previously coated with poly-D-lysine and laminin at 37 °C for 12 h. Cultures were maintained at 37 °C with 5% CO_2 in Neurobasal medium supplemented with 2% B27, 2.5% FBS, and 1×GlutaMAX™-I.

The shRNA sequences were constructed into the pSicoR-Ef1a-mCh-Puro vector (Addgene, #31845), which were verified through Sanger sequencing. Primary neurons were cultured for 14 days and then transfected with the aforementioned constructs (as well as a Venus vector which encodes Venus protein) using Lipofectamine 3000, and were fixed in 4% paraformaldehyde with 4% sucrose after three days. The neurons were stained with antibodies against EGFP and mCherry, and fluorescence positive neurons were randomly selected and their images were captured using an LSM 880 Basic Operation (Carl Zeiss) under consistent acquisition parameters. All assays were blind to experimental conditions in this step.

Dendritic spine analyses were conducted following previous studies [27, 43]. We applied NeuronStudio to analyze spines on secondary and tertiary dendrites [44], and dendrites from one neuron were averaged. Two-tailed student's *t* tests were used to quantify the differences of total dendritic spines between genotypic groups, and two-way ANOVA followed by Bonferroni post-hoc correction was calculated between groups with two independent variables. Results are presented as mean ± SD (Control-shRNA, $n = 70$; *Cnnm2*-shRNA, $n = 74$), and $P \leq 0.05$ was considered as significant.

Proteomics analyses

The identification and quantitation of proteins were performed based on 4D label-free technique with the main procedures as follows. The AAV injected mPFC tissues of mice were dissected and stored as the aforementioned method ($n = 3$, each group). Protein was extracted with SDT (4%SDS, 100 mM Tris-HCl, pH7.6) buffer and digested with trypsin. After desalination, the digest peptides were concentrated by vacuum centrifugation and reconstituted in 0.1% (v/v) formic acid. Then the peptides were subjected to LC-MS/MS analysis on a timsTOF Pro mass spectrometry (Bruker). The MS raw data for each sample were combined and searched using the MaxQuant 1.6.14 software for identification and quantitation analysis. The differentially expressed proteins (DEPs) were selected on the basis of the combination of $|\log_2(\text{fold change})| \geq 1$ and $P \leq 0.05$. Gene ontology (GO) enrichment analysis of the DEPs was performed with Blast2GO [45].

RESULTS

The schizophrenia GWAS risk SNPs at 10q24.32-33 are associated with mRNA and protein levels of *CNNM2* in human DLPFC tissues

We examined the associations of 10q24.32-33 schizophrenia risk SNPs with gene expression using the PsychENCODE DLPFC eQTL dataset ($n = 1387$) [28]. The schizophrenia risk SNPs (e.g., rs11191580 or its LD-index SNPs) were significantly associated with mRNA levels of *CNNM2* in the DLPFC of PsychENCODE sample (Fig. 1B). We also examined the eQTL associations in GTEx dataset, which contains multiple brain and peripheral tissues, and the risk SNP (e.g., rs11191580) was significantly associated with the *CNNM2* mRNA expression only in brain tissues rather than peripheral tissues (Fig. S1). Considering that PsychENCODE and GTEx datasets both primarily comprised of adult individuals, we then examined whether rs11191580 was also associated with *CNNM2* mRNA expression in fetal brains or early developmental stage cells (e.g., neural progenitor cells and neurons) [46–50], but the SNP did not show any evidence of association with *CNNM2* in either database (all $P > 0.05$), suggesting that the eQTL associations were evident only in adults.

Compared to mRNAs, proteins are the eventual products of gene expression and the primary functional components in the molecular processes of cells [51], and integrative analyses combining pQTL and GWAS of brain disorders (e.g., Alzheimer's disorders and depression) have revealed causal brain proteins in the illnesses [32, 52, 53]. We then utilized two independent DLPFC pQTL datasets ($n = 376$ for ROSMAP and $n = 152$ for Banner) [32] to identify proteins whose abundances were correlated with those risk SNPs, and again observed that the protein levels of CNNM2 showed significant associations (Fig. 1C, D).

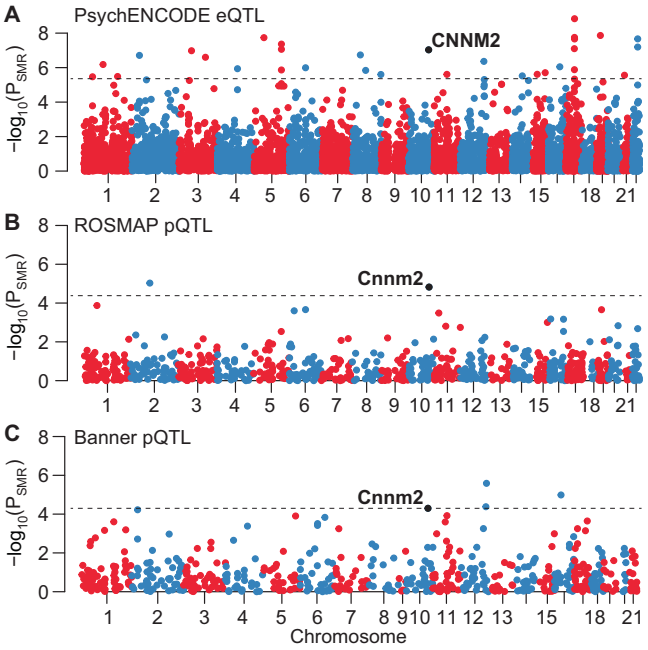

Fig. 2 SMR analyses through integrating schizophrenia PGC3 GWAS with different brain QTL datasets. A PsychENCODE DLPFC eQTL dataset, **B** ROSMAP DLPFC pQTL dataset, **C** Banner DLPFC pQTL dataset. CNNM2 is marked in black. Like Mendelian randomization (MR), the SMR use genetic variants (SNPs) as instrumental variable to test for the causative effect of an exposure (in this study, in refers to gene expression) on an outcome (schizophrenia).

Integrative analyses of DLPFC eQTL and pQTL datasets confirm *CNNM2* as a schizophrenia risk gene

We then performed SMR analyses integrating schizophrenia PGC3 GWAS and DLPFC eQTL/pQTL datasets to identify risk genes at 10q24.32-33 whose mRNA/protein levels were affected by genetic risk of schizophrenia. In the DLPFC eQTL datasets from PsychENCODE [28], lower mRNA levels of *CNNM2* were significantly associated with increased genetic risk of schizophrenia ($P_{SMR} = 9.29 \times 10^{-8}$, $P_{HEIDI} = 0.276$, Fig. 2A). In the independent DLPFC pQTL datasets from ROSMAP [32] and Banner [54], reduced protein levels of CNNM2 were also significantly associated with elevated genetic risk of schizophrenia (ROSMAP, $P_{SMR} = 1.50 \times 10^{-5}$, $P_{HEIDI} = 0.637$, Fig. 2B; Banner, $P_{SMR} = 5.01 \times 10^{-5}$, $P_{HEIDI} = 0.989$, Fig. 2C). Notably, *CNNM2* was the only schizophrenia risk gene showing significance that survived multiple corrections at both mRNA and protein levels, and modulation of *CNNM2* expression likely explain part of the biological impact of schizophrenia risk in the 10q24.32-33 region.

Temporal-spatial expression profiling of *CNNM2* in human tissues and cells

CNNM2 encodes a magnesium transporter playing essential roles in magnesium homeostasis [55, 56]. To specifically explore how *CNNM2* dysfunction contributes to schizophrenia, we firstly investigated the temporal-spatial expression pattern of *CNNM2* in human tissues and cells. According to the GTEx dataset [35], *CNNM2* was highly and widely expressed in human brain tissues including cerebellum and frontal cortex, whereas *CNNM2* mRNA levels were generally low in peripheral tissues (Fig. S2). By analyzing the temporal expression of *CNNM2* using PsychENCODE dataset [28], we found that *CNNM2* expression in brain was slightly

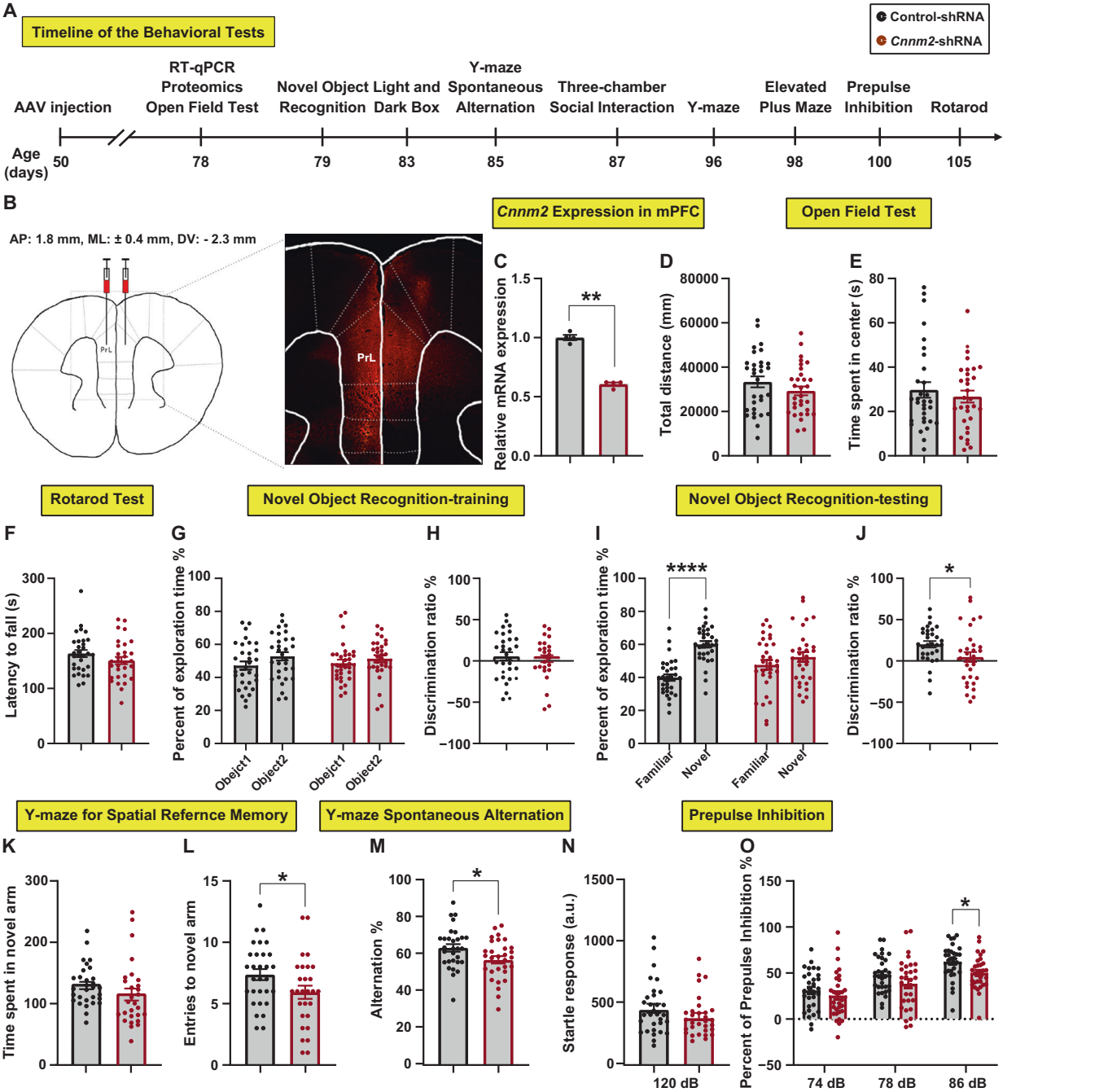

Fig. 3 Knockdown of *Cnnm2* in the mPFC of mice results in behavioral abnormalities associated with schizophrenia. A Timeline of the behavioral tests. **B** Schematic illustration of stereotaxic injection of AAV-*Cnnm2*-shRNA or AAV-Control-shRNA in mPFC (left), and representative image showing red fluorescent protein expression at the injection sites (right). **C** Verification of *Cnnm2* knockdown efficiency by AAV expressing shRNA targeting *Cnnm2*. RT-qPCR showed significantly reduced *Cnnm2* expression in the mPFC of mice injected with AAV-*Cnnm2*-ShRNA compared with the mice injected with AAV-Control-shRNA. $n = 4$ per group, two-tailed student's *t* tests. **D**–**O** Behavioral performance of the control and *Cnnm2* knockdown mice. Two-tailed student's *t* tests. **D**, **E** Open field test. Total distance traveled in the open field apparatus (**D**) and the time spent in the center area (**E**); $n = 31$ per group. **F** Rotarod test. The latency of mice to fall off the rotarod; $n = 31$ per group. **G**–**J** Novel object recognition test. The percent of time spent in exploration of two identical objects separately (**G**) and the discrimination ratio of mice to object 2 (**H**) in the training session. The percent of time spent in exploration of the familiar and novel objects separately (**I**) and the discrimination ratio of mice to the novel object (**J**) in the testing session; $n = 31$ per group. **K**, **L** Y-maze test for spatial reference memory. The time spent in the novel arm (**K**) and the number of entries into the novel arm (**L**); Control-shRNA, $n = 30$; *Cnnm2*-shRNA, $n = 28$. **M** Y-maze spontaneous alteration test. The alteration rate of mice for three consecutive entries to the different arms; $n = 30$ per group. **N**, **O** Prepulse inhibition test. The startle response of the mice to 120 dB pulse stimulus (**N**) and the inhibition of the mice startle response to 120 dB pulse stimulus by prepulse (74 dB, 78 dB, 86 dB) (**O**); $n = 31$ per group. $^{*}P < 0.05$, $^{**}P < 0.01$, $^{****}P < 0.0001$. Error bars indicated standard error of mean. Abbreviations: AP anteroposterior, ML mediolateral, DV dorsoventral, PrL prelimbic cortex.

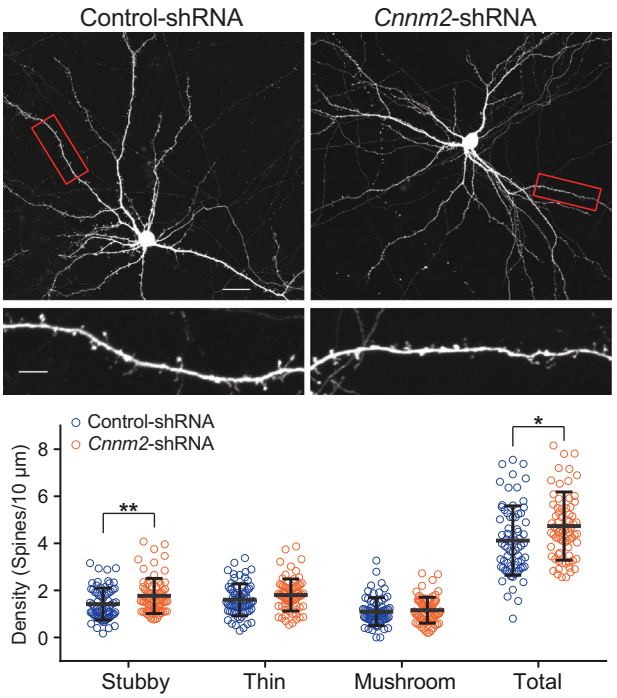

Fig. 4 Knockdown of *Cnnm2* expression in rat primary cortical neurons and their impacts on dendritic spine morphogenesis (*n* ≥ 70 neurons in each experimental group). Confocal images of whole neurons transfected with Control-shRNA or *Cnnm2*-shRNA, and scale bars represent 20 μm. Dendritic branches were from each corresponding neuron respectively, and scale bars represent 5 μm. Neuronal morphologies were visualized by staining for Enhanced Green Fluorescent Protein (EGFP). All neuronal experiments were replicated at least twice with consistent conduct and acquisition parameters, and within each experiment the dendritic spines were counted for each condition from more than three separate cultures. *$P \le 0.05$, **$P \le 0.01$. Error bars indicated standard deviation.

increased after birth compared to that in fetal stages, and remained relatively unchanged throughout postnatal to adult stages (Fig. S3). Notably, comparisons of *CNNM2* mRNA levels in different types of brain cells [28] revealed that the expression of this gene was higher in neurons at the adult stage than that at the developmental stage and the non-neuronal cells (Fig. S4).

Knockdown of *Cnnm2* in the mPFC of mice leads to cognitive impairment and reduces prepulse inhibition

The human DLPFC and its rodent equivalent medial PFC (mPFC) have been implicated in the behavioral abnormalities associated with schizophrenia [57]. The above expression analyses indicate that decreased expression of *CNNM2* in DLPFC was associated with an increased risk of schizophrenia. We then evaluated whether reduced *Cnnm2* expression in mPFC would affect murine behaviors relevant to schizophrenia. We reduced the *Cnnm2* expression in the mPFC of 7-week-old wild-type C57BL/6J male mice through AAV injection, and the timeline of behavioral tests was shown in Fig. 3A. The stereotaxic injection of AAV in mice mPFC was verified at the end of the behavioral tests, and we found that the red fluorescent protein was mainly restricted to the PrL (prelimbic cortex, the targeted brain region) (Fig. 3B). The knockdown efficiency of *Cnnm2* by AAV was confirmed by RT-qPCR. Compared to control group, the expression of *Cnnm2* in mPFC of mice was significantly decreased in *Cnnm2*-shRNA group (Fig. 3C).

Before the behavioral test, all the tested mice had no obvious health problem, such as weight loss or microbial infection. In the open field test, there was no significant difference in total traveled distance and time spent in center area between *Cnnm2* knockdown mice and control mice (total distance, $P = 0.207$; time spent in center, $P = 0.496$, Fig. 3D, E). We then assessed the effect of *Cnnm2* knockdown on the motor and coordination of mice by rotarod test, and demonstrated that the *Cnnm2* knockdown mice exhibited normal motor and coordination function (latency to fall, $P = 0.180$, Fig. 3F). In the light and dark box, the mice with decreased *Cnnm2* showed no significant change in the entries to the light box and the time spent in the light box compared with control mice (entries to the light box, $P = 0.264$; time spent in the light box, $P = 0.979$, Fig. S5A, B). In the elevated plus maze, there was also no difference in the time spent in the open arms and the distance traveled in the open arms between experimental groups (time spent in the open arms, $P = 0.716$; distance traveled in the open arms, $P = 0.677$, Fig. S5C, D). These results indicated that *Cnnm2* expression reduction in mPFC of mice did not lead to anxiety-like behavior.

In the behavioral tests for assessment of recognition memory, there was no significant difference in the time of exploring two identical objects for the *Cnnm2* knockdown mice and control mice (percent of exploration time of Control-shRNA, $P = 0.095$; percent of exploration time of *Cnnm2*-shRNA, $P = 0.420$, Fig. 3G), and the discrimination rate between two groups also showed no significant difference on training session (discrimination ratio, $P = 0.663$, Fig. 3H); the control mice spent significantly more time exploring the novel object than the familiar one, whereas the *Cnnm2* knockdown mice did not (percent of exploration time of Control-shRNA, $P < 0.0001$; percent of exploration time of *Cnnm2*-shRNA, $P = 0.194$, Fig. 3I), and the discrimination to the novel object was significantly decreased when *Cnnm2* was repressed (discrimination ratio, $P = 0.036$, Fig. 3J). These results suggest that reducing *Cnnm2* expression in mice may impair recognition memory. Moreover, we assessed the spatial memory of mice using the Y-maze test, although there was no statistical difference in the time spent in the novel arm (time spent in novel arm, $P = 0.223$, Fig. 3K), the entries of the *Cnnm2* knockdown mice were markedly reduced compared to the control mice (entries to novel arm, $P = 0.045$, Fig. 3L). Furthermore, the spontaneous alternation rate in *Cnnm2* knockdown mice was significantly lower than control mice (alternation, $P = 0.027$, Fig. 3M). In addition, we found that both groups spent more time exploring the strange mouse than the empty enclosure (percent of exploration time of Control-shRNA, $P < 0.0001$; percent of exploration time of *Cnnm2*-shRNA, $P < 0.0001$, Fig. S5E) and the familiar mouse (percent of exploration time of Control-shRNA, $P = 0.056$; percent of exploration time of *Cnnm2*-shRNA, $P = 0.004$, Fig. S5G) in the three-chambered social interaction test, and there was no difference in the discrimination ratio between two groups on both stages (discrimination ratio of stage 2, $P = 0.874$; discrimination ratio of stage 3, $P = 0.612$, Fig. S5F, H), indicating that the *Cnnm2* knockdown mice showed normal social interest and social novelty. Taken together, these results indicated that knockdown of *Cnnm2* in mPFC of mice led to cognitive impairment.

In the PPI test, no differences in amplitude of the startle response at 120 dB were observed between mice of different experimental groups (startle response, $P = 0.166$, Fig. 3N). We hence continued to evaluate sensorimotor gating, measured as a reduction of the acoustic startle response after prepulse exposure. Notably, the mice with reduced *Cnnm2* exhibited significantly attenuated inhibition in response to the startle pulse when given the 86 dB pre-pulse (percent of PPI-74 dB, $P = 0.323$; percent of PPI-78 dB, $P = 0.079$; percent of PPI-86 dB, $P = 0.031$, Fig. 3O). This indicated that the sensorimotor gating function of mice was compromised by the suppression of *Cnnm2*.

Knockdown of *Cnnm2* in primary neurons affects dendritic spine morphogenesis

We transfected *Cnnm2*-shRNA construct in cortical neurons to reduce the expression of *Cnnm2*, which corroborated a higher

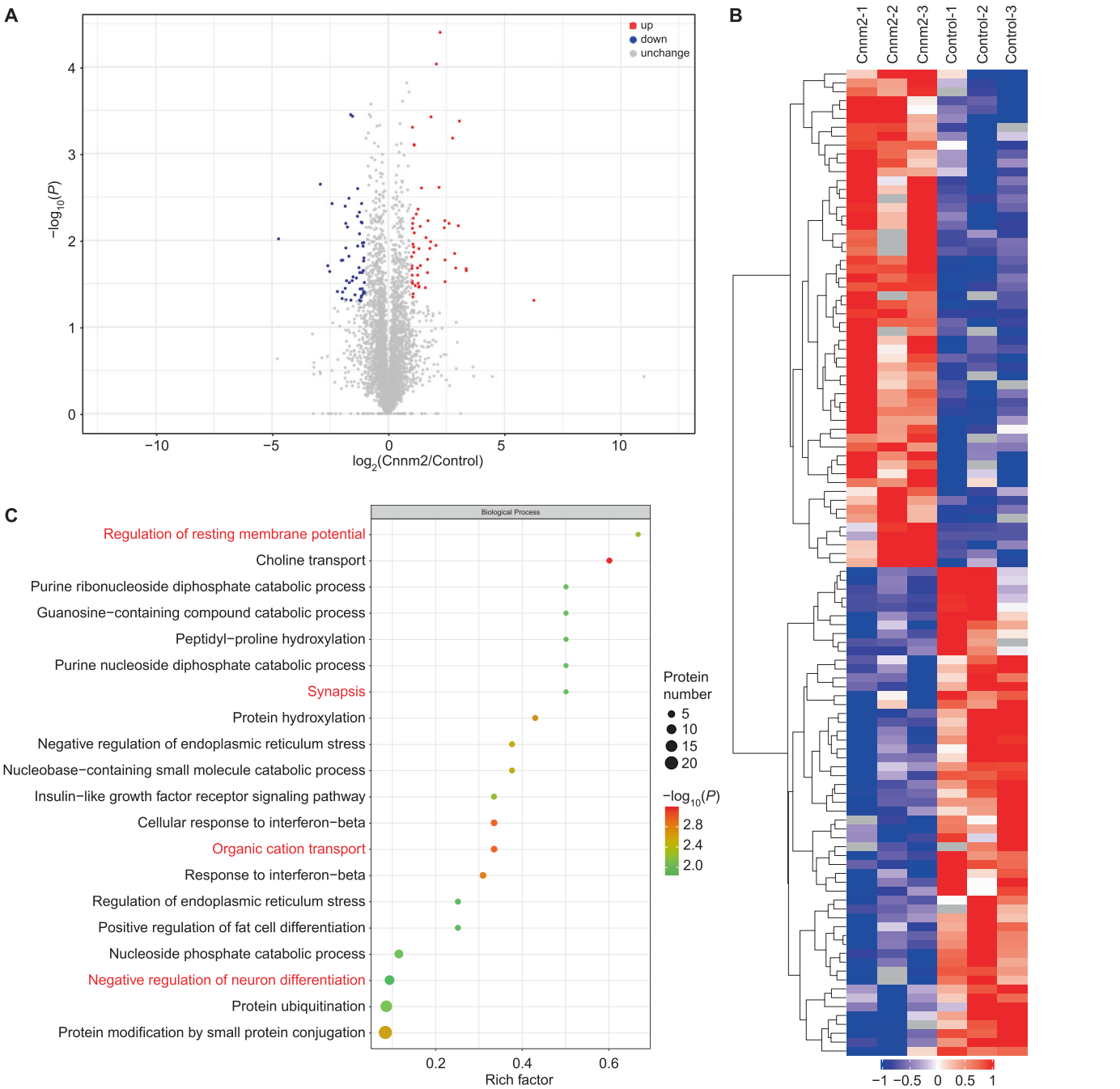

Fig. 5 overview of the altered proteome of mPFC in *Cnnm2* knockdown mice. A Volcano plot of differentially expressed proteins, $|\log_2(\text{fold change})| > 1$, $P < 0.05$. **B** Hierarchical clustering analysis of all identified differentially expressed proteins and the corresponding Heatmap. Red: upregulated. Blue: downregulated. The color in the Heatmap indicates the protein expression level which was scaled across all samples and displayed as Z-score. **C** The top GO enrichment of biological process of all identified differentially expressed proteins. The circle size represents the number of proteins enriched in each item.

genetic risk of schizophrenia. The knockdown efficiencies of *Cnnm2* by shRNA constructs were confirmed (Fig. S6). We observed significant increased total spine density in *Cnnm2* knockdown neurons compared with control neurons (Control-shRNA, 4.121 ± 1.476 spines per 10 μm; *Cnnm2*-shRNA, 4.735 ± 1.449 spines per 10 μm; $P = 0.0129$; Fig. 4). Further post-hoc multiple comparisons showed that suppression of *Cnnm2* leads to a significantly increased density of stubby dendritic spines (Control-shRNA, 1.422 ± 0.678 spines per 10 μm; *Cnnm2*-shRNA, 1.768 ± 0.746 spines per 10 μm; $P = 0.0053$; Fig. 4), while the densities of thin or mushroom spines were not affected.

Decreased *Cnnm2* level causes changed expression of proteins associated with neuronal function

We then investigated the molecular changes in mPFC induced by decreased *Cnnm2* levels through proteomic analysis. In brief, 111 proteins were identified differentially expressed ($|\log_2(\text{fold change})| \geq 1$ and $P \leq 0.05$) in *Cnnm2* knockdown mice compared with controls (Fig. 5A, B, Table S1). Among these DEPs, 16 DEPs

were involved in synaptic plasticity regulation or ion channel formation (Table S2), for example, Neuronal pentraxin-2 (encoded by *Nptx2*) enhances the accumulation of AMPARs on the postsynaptic membranes [58], and Girdin (encoded by *Ccdc88a*) regulates NMDAR activation associated with neuronal plasticity [59]. GO enrichment analysis showed that the DEPs were significantly enriched in the biological processes related to neuronal structure and function, resting membrane potential, and organic cation transport (Fig. 5C).

DISCUSSION

Accumulating GWAS have reported hundreds of genomic loci associated with clinical diagnosis of schizophrenia, and the 10q24.32-33 locus has been consistently characterized as one of the most significant genomic loci. Here, we reported an important schizophrenia risk gene *CNNM2* in the 10q24.32-33 region, and its reduced mRNA and protein expression in DLPFC tissues predicted higher genetic risk of the illness in Europeans. Intriguingly, *CNNM2* was also highlighted in a SMR analysis integrating schizophrenia GWAS and prefrontal cortex eQTL dataset in East Asian populations [60], suggesting that this gene was likely involved in schizophrenia across different ethnic populations. Another study of phenotype atlas for abnormal behavior and brain activity in zebrafish mutants also reported that Cnnm2 was a potential driver of the schizophrenia risk associations at 10q24.32-33 [61]. These lines of evidence suggest pivotal roles of *CNNM2* in schizophrenia pathogenesis, and it is of great interest to explore the function of this risk gene in brain development. In the present study, we have demonstrated that reduced *Cnnm2* in the mPFC of mice could lead to cognitive impairment and sensorimotor gating deficit (an endophenotype of schizophrenia). Since *CNNM2* plays essential roles in the homeostasis of magnesium [55], an essential regulator in neuronal maturation and neuropathology [56], our discovery may be related to the dysfunction of *CNNM2* in transporting Magnesium ion (Mg^{2+}). Mg^{2+} is a highly selective inhibitor of NMDA receptor, and the Mg^{2+} homeostasis is essential for the activity of NMDAR [62]. The long-term potentiation and long-term depression induced by NMDAR stimulation are the most important mechanisms of synaptic plasticity, which plays crucial roles in the process of learning and memory formation [63]. Notably, we have shown that reduced *Cnnm2* affected dendritic spine morphogenesis, and abnormal expression of proteins involved in synaptic plasticity regulation or ion channel formation. Therefore, decreased *Cnnm2* in mPFC may induce sensorimotor gating dysfunction through affecting Mg^{2+} homeostasis, NMDAR activity and synaptic plasticity.

However, cautions should also be kept given some inconsistent observations, for example, previous studies found reduced dendritic spines in the brains of schizophrenia patients [17, 20], while our study found that higher genetic risk of *CNNM2* predicted increased stubby dendritic spines. Stubby spines are prevalent in the early stages of postnatal development and their number declines during the brain maturation [64, 65]. They lack distinctive head and neck, and are less mature compared with mushroom spines and likely represent the transient stages of spine formation and elimination [66], whereas an over-representation of the less mature spines is likely to cause impaired cognitive functions [67]. Although there is a general consensus that schizophrenia was associated with decreases in dendritic spine density [17, 20, 23, 68], there are still obstacles and challenges to the dendritic spine pathology hypothesis of schizophrenia. One crucial issue is that the findings of reduced density of dendritic spines in schizophrenia were identified in postmortem brain tissue, a result inevitably affected by some confounding factors including antipsychotics treatment, duration and severity of illness, tobacco and alcohol use, and drug abuse [69]. It is thus difficult to simulate this time-dependent developmental changes with primary neurons cultured in vitro. In addition, there were also studies reporting that schizophrenia risk genes lead to an increased density of immature spines and impaired synaptic function in primary cortical neurons or in the rodent PFC. For example, Kristina et al. have reported that increased nitric oxide synthase 1 adapter protein (encoded by a schizophrenia risk gene *NOS1AP* [70]) promoted the formation of immature spines in primary rat cortical neurons and influenced synaptic function [71]. Expression and activity of the phosphoinositide 3-kinase (PI3K) catalytic isoform, PIK3CD/p110δ, is increased in schizophrenia, and overexpression of p110δ in primary rat hippocampal cultures significantly increased immature and mature dendritic spine densities [72]. Moreover, *Tcf4tg* mice, the transgenic mice overexpressing transcription factor 4 (encoded by a schizophrenia risk gene *TCF4* [2]) in forebrain, showed higher density of immature (stubby) spines during development and displayed deficits in sensorimotor gating [73]. Therefore, increased density of stubby spines is not equivalent to enhanced synaptic plasticity and better cognitive function, and our results indicate that knockdown of *Cnnm2* in primary neurons may affect neuronal development and may be involved in impaired cognitive functions.

In addition, we acknowledge another potential limitation that it would be best to perform the behavioral analyses and spine density experiment both in mice. Nevertheless, there has been studies showing that manipulation of schizophrenia risk genes lead to consistent spine phenotypes in rat and mice primary neurons, for example, knockdown of *Zfp804a* could decrease the dendritic spine density both in primary rat cortical neurons and mouse cortical neurons [13, 26, 74]. In addition, since *Cnnm2* is highly conserved across rat and mice (~99.4%), the effects of this gene on the dendritic spine morphogenesis of rat and mouse neurons might be consistent.

In conclusion, we have characterized a schizophrenia risk gene *CNNM2*. Its critical functional impact on sensorimotor gating function and dendritic spine morphogenesis highlights its putative involvement in schizophrenia pathogenesis. Further studies are warranted to explore the effect of decreased *CNNM2* expression on synaptic function to illustrate the detailed mechanism of this gene in schizophrenia.

REFERENCES

1. Sullivan PF, Kendler KS, Neale MC. Schizophrenia as a complex trait: evidence from a meta-analysis of twin studies. Arch Gen Psychiatry. 2003;60:1187–92.
2. Trubetskoy V, Pardinas AF, Qi T, Panagiotaropoulou G, Awasthi S, Bigdeli TB, et al. Mapping genomic loci implicates genes and synaptic biology in schizophrenia. Nature. 2022;604:502–8.
3. Edwards SL, Beesley J, French JD, Dunning AM. Beyond GWASs: illuminating the dark road from association to function. Am J Hum Genet. 2013;93:779–97.
4. Gusev A, Mancuso N, Won H, Kousi M, Finucane HK, Reshef Y, et al. Transcriptome-wide association study of schizophrenia and chromatin activity yields mechanistic disease insights. Nat Genet. 2018;50:538–48.
5. Huckins LM, Dobbyn A, Ruderfer DM, Hoffman G, Wang W, Pardinas AF, et al. Gene expression imputation across multiple brain regions provides insights into schizophrenia risk. Nat Genet. 2019;51:659–74.
6. Fromer M, Roussos P, Sieberts SK, Johnson JS, Kavanagh DH, Perumal TM, et al. Gene expression elucidates functional impact of polygenic risk for schizophrenia. Nat Neurosci. 2016;19:1442–53.
7. Jaffe AE, Straub RE, Shin JH, Tao R, Gao Y, Collado-Torres L, et al. Developmental and genetic regulation of the human cortex transcriptome illuminate schizophrenia pathogenesis. Nat Neurosci. 2018;21:1117–25.
8. Schizophrenia Psychiatric Genome-Wide Association Study Consortium. Genome-wide association study identifies five new schizophrenia loci. Nat Genet. 2011;43:969–76.
9. Schizophrenia Working Group of the Psychiatric Genomics Consortium. Biological insights from 108 schizophrenia-associated genetic loci. Nature. 2014;511:421–7.

10. Wynn JK, Dawson ME, Schell AM, McGee M, Salveson D, Green MF. Prepulse facilitation and prepulse inhibition in schizophrenia patients and their unaffected siblings. Biol Psychiatry. 2004;55:518–23.
11. San-Martin R, Castro LA, Menezes PR, Fraga FJ, Simoes PW, Salum C. Meta-analysis of sensorimotor gating deficits in patients with schizophrenia evaluated by prepulse inhibition test. Schizophr Bull. 2020;46:1482–97.
12. Swerdlow NR, Weber M, Qu Y, Light GA, Braff DL. Realistic expectations of prepulse inhibition in translational models for schizophrenia research. Psychopharmacology (Berl). 2008;199:331–88.
13. Huang Y, Huang J, Zhou QX, Yang CX, Yang CP, Mei WY, et al. ZFP804A mutant mice display sex-dependent schizophrenia-like behaviors. Mol Psychiatry. 2021;26:2514–32.
14. Miro X, Meier S, Dreisow ML, Frank J, Strohmaier J, Breuer R, et al. Studies in humans and mice implicate neurocan in the etiology of mania. Am J Psychiatry. 2012;169:982–90.
15. Carr GV, Chen J, Yang F, Ren M, Yuan P, Tian Q, et al. KCNH2-3.1 expression impairs cognition and alters neuronal function in a model of molecular pathology associated with schizophrenia. Mol Psychiatry. 2016;21:1517–26.
16. Weinberger DR. Implications of normal brain development for the pathogenesis of schizophrenia. Arch Gen Psychiatry. 1987;44:660–9.
17. Glantz LA, Lewis DA. Decreased dendritic spine density on prefrontal cortical pyramidal neurons in schizophrenia. Arch Gen Psychiatry. 2000;57:65–73.
18. Osimo EF, Beck K, Reis Marques T, Howes OD. Synaptic loss in schizophrenia: a meta-analysis and systematic review of synaptic protein and mRNA measures. Mol Psychiatry. 2019;24:549–61.
19. Berdenis van Berlekom A, Muflihah CH, Snijders G, MacGillavry HD, Middeldorp J, Hol EM, et al. Synapse pathology in schizophrenia: a meta-analysis of postsynaptic elements in postmortem brain studies. Schizophr Bull. 2020;46:374–86.
20. MacDonald ML, Alhassan J, Newman JT, Richard M, Gu H, Kelly RM, et al. Selective loss of smaller spines in schizophrenia. Am J Psychiatry. 2017;174:586–94.
21. Penzes P, Cahill ME, Jones KA, VanLeeuwen JE, Woolfrey KM. Dendritic spine pathology in neuropsychiatric disorders. Nat Neurosci. 2011;14:285–93.
22. Forrest MP, Parnell E, Penzes P. Dendritic structural plasticity and neuropsychiatric disease. Nat Rev Neurosci. 2018;19:215–34.
23. Glausier JR, Lewis DA. Dendritic spine pathology in schizophrenia. Neuroscience. 2013;251:90–107.
24. Smith KR, Kopeikina KJ, Fawcett-Patel JM, Leaderbrand K, Gao R, Schurmann B, et al. Psychiatric risk factor ANK3/ankyrin-G nanodomains regulate the structure and function of glutamatergic synapses. Neuron. 2014;84:399–415.
25. Hayashi-Takagi A, Takaki M, Graziane N, Seshadri S, Murdoch H, Dunlop AJ, et al. Disrupted-in-Schizophrenia 1 (DISC1) regulates spines of the glutamate synapse via Rac1. Nat Neurosci. 2010;13:327–32.
26. Deans PJM, Raval P, Sellers KJ, Gatford NJF, Halai S, Duarte RRR, et al. Psychosis risk candidate ZNF804A localizes to synapses and regulates neurite formation and dendritic spine structure. Biol Psychiatry. 2017;82:49–61.
27. Zhou D, Xiao X, Li M. The schizophrenia risk isoform ZNF804A^{E3E4} affects dendritic spine. Schizophr Res. 2020;218:324–5.
28. Wang D, Liu S, Warrell J, Won H, Shi X, Navarro FCP, et al. Comprehensive functional genomic resource and integrative model for the human brain. Science. 2018;362:eaat8464.
29. Ongen H, Buil A, Brown AA, Dermitzakis ET, Delaneau O. Fast and efficient QTL mapper for thousands of molecular phenotypes. Bioinformatics. 2016;32:1479–85.
30. Stegle O, Parts L, Durbin R, Winn J. A Bayesian framework to account for complex non-genetic factors in gene expression levels greatly increases power in eQTL studies. PLoS Comput Biol. 2010;6:e1000770.
31. Purcell S, Neale B, Todd-Brown K, Thomas L, Ferreira MA, Bender D, et al. PLINK: a tool set for whole-genome association and population-based linkage analyses. Am J Hum Genet. 2007;81:559–75.
32. Wingo AP, Liu Y, Gerasimov ES, Gockley J, Logsdon BA, Duong DM, et al. Integrating human brain proteomes with genome-wide association data implicates new proteins in Alzheimer's disease pathogenesis. Nat Genet. 2021;53:143–6.
33. Robins C, Liu Y, Fan W, Duong DM, Meigs J, Harerimana NV, et al. Genetic control of the human brain proteome. Am J Hum Genet. 2021;108:400–10.
34. Zhu Z, Zhang F, Hu H, Bakshi A, Robinson MR, Powell JE, et al. Integration of summary data from GWAS and eQTL studies predicts complex trait gene targets. Nat Genet. 2016;48:481–7.
35. GTEx Consortium. The Genotype-Tissue Expression (GTEx) project. Nat Genet. 2013;45:580–5.
36. Lake BB, Ai R, Kaeser GE, Salathia NS, Yung YC, Liu R, et al. Neuronal subtypes and diversity revealed by single-nucleus RNA sequencing of the human brain. Science. 2016;352:1586–90.
37. Darmanis S, Sloan SA, Zhang Y, Enge M, Caneda C, Shuer LM, et al. A survey of human brain transcriptome diversity at the single cell level. Proc Natl Acad Sci USA. 2015;112:7285–90.
38. Lake BB, Chen S, Sos BC, Fan J, Kaeser GE, Yung YC, et al. Integrative single-cell analysis of transcriptional and epigenetic states in the human adult brain. Nature Biotechnol. 2018;36:70–80.
39. Lei Y, Wang J, Wang D, Li C, Liu B, Fang X, et al. SIRT1 in forebrain excitatory neurons produces sexually dimorphic effects on depression-related behaviors and modulates neuronal excitability and synaptic transmission in the medial prefrontal cortex. Mol Psychiatry. 2020;25:1094–111.
40. Zhang Z, Ye M, Li Q, You Y, Yu H, Ma Y, et al. The schizophrenia susceptibility gene OPCML regulates spine maturation and cognitive behaviors through Eph-Cofilin signaling. Cell Rep. 2019;29:49–61.e47.
41. Cai X, Yang ZH, Li HJ, Xiao X, Li M, Chang H. A human-specific schizophrenia risk tandem repeat affects alternative splicing of a human-unique isoform AS3MT^{d2d3} and mushroom dendritic spine density. Schizophr Bull. 2021;41:219–27.
42. Yang Z, Zhou D, Li H, Cai X, Liu W, Wang L, et al. The genome-wide risk alleles for psychiatric disorders at 3p21.1 show convergent effects on mRNA expression, cognitive function and mushroom dendritic spine. Mol Psychiatry. 2020;25:48–66.
43. Srivastava DP, Woolfrey KM, Penzes P. Analysis of dendritic spine morphology in cultured CNS neurons. J Vis Exp. 2011;53:e2794.
44. Rodriguez A, Ehlenberger DB, Dickstein DL, Hof PR, Wearne SL. Automated three-dimensional detection and shape classification of dendritic spines from fluorescence microscopy images. PLoS One. 2008;3:e1997.
45. Conesa A, Gotz S, Garcia-Gomez JM, Terol J, Talon M, Robles M. Blast2GO: a universal tool for annotation, visualization and analysis in functional genomics research. Bioinformatics. 2005;21:3674–6.
46. O'Brien HE, Hannon E, Hill MJ, Toste CC, Robertson MJ, Morgan JE, et al. Expression quantitative trait loci in the developing human brain and their enrichment in neuropsychiatric disorders. Genome Biol. 2018;19:194.
47. Jerber J, Seaton DD, Cuomo ASE, Kumasaka N, Haldane J, Steer J, et al. Population-scale single-cell RNA-seq profiling across dopaminergic neuron differentiation. Nat Genet. 2021;53:304–12.
48. Bryois J, Calini D, Macnair W, Foo L, Urich E, Ortmann W, et al. Cell-type-specific cis-eQTLs in eight human brain cell types identify novel risk genes for psychiatric and neurological disorders. Nat Neurosci. 2022;25:1104–12.
49. Aygun N, Elwell AL, Liang D, Lafferty MJ, Cheek KE, Courtney KP, et al. Brain-trait-associated variants impact cell-type-specific gene regulation during neurogenesis. Am J Hum Genet. 2021;108:1647–68.
50. Walker RL, Ramaswami G, Hartl C, Mancuso N, Gandal MJ, de la Torre-Ubieta L, et al. Genetic control of expression and splicing in developing human brain informs disease mechanisms. Cell. 2019;179:750–771.e722.
51. Vogel C, Marcotte EM. Insights into the regulation of protein abundance from proteomic and transcriptomic analyses. Nat Rev Genet. 2012;13:227–32.
52. Wingo TS, Liu Y, Gerasimov ES, Gockley J, Logsdon BA, Duong DM, et al. Brain proteome-wide association study implicates novel proteins in depression pathogenesis. Nat Neurosci. 2021;24:810–7.
53. Liu J, Li X, Luo XJ. Proteome-wide association study provides insights into the genetic component of protein abundance in psychiatric disorders. Biol Psychiatry. 2021;90:781–9.
54. Padmanabhan S, Dominiczak AF. Genomics of hypertension: the road to precision medicine. Nat Rev Cardiol. 2021;18:235–50.
55. Arjona FJ, de Baaij JH, Schlingmann KP, Lameris AL, van Wijk E, Flik G, et al. CNNM2 mutations cause impaired brain development and seizures in patients with hypomagnesemia. PLoS Genet. 2014;10:e1004267.
56. Yamanaka R, Shindo Y, Oka K. Magnesium is a key player in neuronal maturation and neuropathology. Int J Mol Sci. 2019;20:3439.
57. Moghaddam B, Homayoun H. Divergent plasticity of prefrontal cortex networks. Neuropsychopharmacology. 2008;33:42–55.
58. Goverti D, Buyukluoglu N, Kaya H, Yuksel RN, Yucel C, Goka E. Neuronal pentraxin-2 (NPTX2) serum levels during an acute psychotic episode in patients with schizophrenia. Psychopharmacology (Berl). 2022;239:2585–91.
59. Nakai T, Nagai T, Tanaka M, Itoh N, Asai N, Enomoto A, et al. Girdin phosphorylation is crucial for synaptic plasticity and memory: a potential role in the interaction of BDNF/TrkB/Akt signaling with NMDA receptor. J Neurosci. 2014;34:14995–5008.
60. Liu S, Chen Y, Wang F, Jiang Y, Duan F, Xia Y, et al. Brain transcriptional regulatory architecture and schizophrenia etiology converge between East Asian and European ancestral populations. 2021. bioRxiv: https://doi.org/10.1101/2021.02.04.922880.
61. Thyme SB, Pieper LM, Li EH, Pandey S, Wang Y, Morris NS, et al. Phenotypic landscape of schizophrenia-associated genes defines candidates and their shared functions. Cell. 2019;177:478–91.e420.
62. Collingridge GL, Abraham WC. Glutamate receptors and synaptic plasticity: the impact of Evans and Watkins. Neuropharmacology. 2022;206:108922.
63. Lynch MA. Long-term potentiation and memory. Physiol Rev. 2004;84:87–136.
64. Harris KM, Jensen FE, Tsao B. Three-dimensional structure of dendritic spines and synapses in rat hippocampus (CA1) at postnatal day 15 and adult ages:

implications for the maturation of synaptic physiology and long-term potentiation. J Neurosci. 1992;12:2685–705.
65. Hering H, Sheng M. Dendritic spines: structure, dynamics and regulation. Nat Rev Neurosci. 2001;2:880–8.
66. Helm MS, Dankovich TM, Mandad S, Rammner B, Jähne S, Salimi V, et al. A large-scale nanoscopy and biochemistry analysis of postsynaptic dendritic spines. Nat Neurosci. 2021;24:1151–62.
67. Sanchez-Gonzalez A, Thougaard E, Tapias-Espinosa C, Canete T, Sampedro-Viana D, Saunders JM, et al. Increased thin-spine density in frontal cortex pyramidal neurons in a genetic rat model of schizophrenia-relevant features. Eur Neuropsychopharmacol. 2021;44:79–91.
68. Glantz LA, Lewis DA. Dendritic spine density in schizophrenia and depression. Arch Gen Psychiatry. 2001;58:203.
69. Li W, Lv L, Luo XJ. In vivo study sheds new light on the dendritic spine pathology hypothesis of schizophrenia. Mol Psychiatry. 2022;27:1866–8.
70. Wratten NS, Memoli H, Huang Y, Dulencin AM, Matteson PG, Cornacchia MA, et al. Identification of a schizophrenia-associated functional noncoding variant in NOS1AP. Am J Psychiatry. 2009;166:434–41.
71. Hernandez K, Swiatkowski P, Patel MV, Liang C, Dudzinski NR, Brzustowicz LM, et al. Overexpression of isoforms of nitric oxide synthase 1 adaptor protein, encoded by a risk gene for schizophrenia, alters actin dynamics and synaptic function. Front Cell Neurosci. 2016;10:6.
72. Hood VL, Paterson C, Law AJ. PI3Kinase-p110delta overexpression impairs dendritic morphogenesis and increases dendritic spine density. Front Mol Neurosci. 2020;13:29.
73. Badowska DM, Brzozka MM, Kannaiyan N, Thomas C, Dibaj P, Chowdhury A, et al. Modulation of cognition and neuronal plasticity in gain- and loss-of-function mouse models of the schizophrenia risk gene Tcf4. Transl Psychiatry. 2020;10:343.
74. Dong F, Mao J, Chen M, Yoon J, Mao Y. Schizophrenia risk ZNF804A interacts with its associated proteins to modulate dendritic morphology and synaptic development. Mol Brain. 2021;14:12.

ACKNOWLEDGEMENTS

The authors sincerely acknowledge the important contributions of many publicly available datasets, including the PGC, the ROSMAP and Banner, and the PsychENCODE Consortium. We thank the participants of the ROS, MAP, Mayo, Mount Sinai Brain Bank and Banner Sun Health Research Institute Brain and Body Donation Program for their time and participation. Data were generated as part of the PsychENCODE Consortium, supported by: U01MH103392, U01MH103365, U01MH103346, U01MH103340, U01MH103339, R21MH109956, R21MH105881, R21MH105853, R21MH103877, R21MH102791, R01MH111721, R01MH110928, R01MH110927, R01MH110926, R01MH110921, R01MH110920, R01MH110905, R01MH109715, R01MH109677, R01MH105898, R01MH105898, R01MH094714, P50MH106934, U01MH116488, U01MH116487, U01MH116492, U01MH116489, U01MH116438, U01MH116441, U01MH116442, R01MH114911, R01MH114899, R01MH114901, R01MH117293, R01MH117291, R01MH117292 awarded to: Schahram Akbarian (Icahn School of Medicine at Mount Sinai), Gregory Crawford (Duke University), Stella Dracheva (Icahn School of Medicine at Mount Sinai), Peggy Farnham (University of Southern California), Mark Gerstein (Yale University), Daniel Geschwind (University of California, Los Angeles), Fernando Goes (Johns Hopkins University), Thomas M. Hyde (Lieber Institute for Brain Development), Andrew Jaffe (Lieber Institute for Brain Development), James A. Knowles (University of Southern California), Chunyu Liu (SUNY Upstate Medical University), Dalila Pinto (Icahn School of Medicine at Mount Sinai), Panos Roussos (Icahn School of Medicine at Mount Sinai), Stephan Sanders (University of California, San Francisco), Nenad Sestan (Yale University), Pamela Sklar (Icahn School of Medicine at Mount Sinai), Matthew State (University of California, San Francisco), Patrick Sullivan (University of North Carolina), Flora Vaccarino (Yale University), Daniel Weinberger (Lieber Institute for Brain Development), Sherman Weissman (Yale University), Kevin White (University of Chicago), Jeremy Willsey (University of California, San Francisco), and Peter Zandi (Johns Hopkins University).

AUTHOR CONTRIBUTIONS

ML, LXL and MS designed the study and interpreted the results. DYZ, XS and YW performed the primary experiments and analyses. YFY, LWZ, SMC, MLS, WQL, ZHZ and LW contributed to the analyses and results interpretation. DYZ, MS, ML and XS drafted the first manuscript, and all authors contributed to the final version of the paper.

FUNDING

This work was supported by grants from the National Natural Science Foundation of China (U22A20304 and 81971252 to LXL, 82001407 to XS, 32100482 to LW, 81903688 to MLS), Science and Technology Project of Henan Province (212102310587 to MS, 222102310130 to XS), Spring City Plan: the High-level Talent Promotion and Training Project of Kunming (2022SCP001), Yunnan Fundamental Research Projects (202101AT070283 to LW), Youth Project of Medical Science and Technology of Henan Province (SBGJ202103094 to XS), Open Project of Henan Key Laboratory of Biological Psychiatry (ZDSYS2022002 to MS), High Scientific and Technological Research Fund of Xinxiang Medical University (2017ZDCG-04 to LXL), Major Science and Technology Projects of Henan Province (201300310200 to LXL), Project (joint construction) of Medical Science and Technology in Henan Province (LHGJ20190475 to MLS).

COMPETING INTEREST

The authors declare no competing interests.

ADDITIONAL INFORMATION

Supplementary information The online version contains supplementary material available at https://doi.org/10.1038/s41386-023-01732-y.

Correspondence and requests for materials should be addressed to Ming Li or Meng Song.